IEEE Access
Multidisciplinary | Rapid Review | Open Access Journal

Received November 14, 2020, accepted November 29, 2020, date of publication December 4, 2020,
date of current version December 16, 2020.

Digital Object Identifier 10.1109/ACCESS.2020.3042718

Effects of Dispersion and Multi-Path Propagation in Partial Discharges Location

JOAQUÍN GRANADO, ANTONIO TORRALBA, (Senior Member, IEEE), AND CÉSAR ÁLVAREZ-ARROYO
Electronic Engineering Department, ETSI, Universidad de Sevilla, 41092 Sevilla, Spain

Corresponding author: Joaquín Granado (j_granado@us.es)

This work was supported by the Laboratory of Engineering for Energy and Environmental Sustainability, Universidad de Sevilla, under Grant of the VI Plan Propio de Investigación.

ABSTRACT Dispersion and multi-path propagation distort partial discharge (PD) pulses that travel along power cables. This article proposes a theoretical framework that models the PD source location error owing to these effects. Regarding dispersion, a closed-form expression is proposed to estimate the PD bandwidth reduction at the cable ends, as well as the expected location error due to propagation velocity variation. A new expression is proposed for the difference of times of arrival (TOAs), which exhibits dependence with frequency. Multi-path propagation also introduces a non-linear dependence with frequency in the TOAs, which leads to location errors when the echo is very close to the main PD signal. Three location algorithms (based on cross-correlation, phase increment, and energy criterion) are investigated under noise, dispersion, and multi-path conditions. Simulation results show that the energy criterion algorithm is very sensitive to dispersion, but it is robust to multi-path propagation. The algorithm based on phase increments is the most sensitive to noise. Finally, the best location method for noisy, highly dispersive, multi-path propagation is the one based on cross-correlation.

INDEX TERMS Partial discharge, fault location, power cables.

I. INTRODUCTION

The insulation condition of power distribution networks can be continuously monitored by measuring the partial discharge (PD) activity [1], [2]. In medium voltage infrastructure, high PD activity warns that dielectrics in cables, junctions, connectors, or switchgears are being degraded. Eventual destructive breakdowns can be preventively avoided by using accurate location systems during maintenance operation. Modern online maintenance systems allow both, detection and location of PDs, under real operational conditions, avoiding the need to disconnect critical systems components [3]. In medium voltage cables [4], PDs are generated in a degraded site, and propagate along the cable towards both ends, where the monitoring systems are in charge of detecting and locating PD activity.

In medium voltage cables both, the high frequency behaviour of the semiconductor layer [5], and the effects of aging [6], make each frequency component of the PD signal travel with a different propagation velocity. This effect, called dispersion, spreads PD pulses as they travel along the cable [4] and, as a consequence, their bandwidth is reduced. Detection and location systems based on conventional narrow-band sensors are rarely affected by dispersion, since the total available bandwidth is in the range of kHz or, at most, a few MHz. Recent techniques extend the bandwidth of measurements up to hundred of MHz, or even in the GHz range [7]–[11]. In noisy environments, a significant part of the available spectrum acquired by these broad-band sensors is not occupied by the PD signal owing to dispersion, especially in long cables. Dispersion also affects the time of arrival (TOA), which is commonly used to estimate the location of PD sources [12]–[20]. Dispersion changes the PD pulse shape while propagating along the cable.

Although dispersion can be modeled using a classical transmission line approach [21], [22], those models based on transfer function are preferable because no knowledge about the cable geometry or material specification is needed [12], [23]. In this article we use the model proposed in [23], where propagation is modeled by one single parameter,

The associate editor coordinating the review of this manuscript and approving it for publication was Hui Ma.

the dispersion constant, which is easy to measure with a vector network analyzer.

Multi-path propagation degrades the estimation accuracy of the TOA-based location techniques [24]. PD signals suffer severe fading due to the destructive interference of echos [25], especially when the PD source is very close to a cable end (e.g., in connectors). In this situation, a strong echo may occur, and it is difficult to differentiate it from the original PD signal because both signals are close in time.

In this article, the accuracy of double-ended TOA-based location methods under dispersion and multi-path propagation conditions is analyzed. Next list itemizes the contributions of this article:

- A new closed-form expression to estimate the bandwidth reduction suffered by PD pulses due to dispersion is proposed. Since noise is the main problem for on-line PD detection and location [26], such an expression is useful to select the most appropriate bandwidth for measurements. This selection allows location and detection algorithms to work with signals of a higher signal-to-noise ratio (SNR), which is especially important for those using broadband sensors.
- Theoretical expressions to calculate a lower bound of the location error due to dispersion and multi-path propagation are proposed. These new expressions provide us with a better understanding the impact of dispersion and multi-path propagation on the accuracy of location techniques.
- The accuracy of three conventional location techniques: cross-correlation in the time domain [14], phase increments in the frequency domain [13], and one technique based on an energy function [27], is assessed by means of simulation. Dispersion and multi-path propagation are shown to produce different effects in these localization techniques. This analysis helps engineers better understand the maximum achievable location accuracy, and select the most appropriate technique for a given propagation conditions.

This article is organized into four additional sections. Section II presents the propagation model and proposes some new expressions to model the effects of dispersion and multi-path propagation. Section III describes the location methods whose accuracy will be investigated. Section IV presents some simulation results under different propagation conditions. Finally, in Section V, some conclusions are drawn.

II. PROPAGATION EFFECTS ON LOCATION ERROR

A. PROPAGATION MODEL

Fig. 1 shows the reference model under consideration. A PD pulse, labeled $x_0(t)$, is generated in the degraded area, and travels simultaneously towards the near- and far- ends of the cable, resulting in two signals: $x_1(t)$ at the near-end, and $x_2(t)$ at the far-end.

The transfer function $H(\omega, L)$, shown in (1), was proposed in [23] to model the propagation of PDs in medium voltage cables. In (1), α_0 and $\beta(\omega)$ are the real and the imaginary parts, respectively, of the propagation constant.

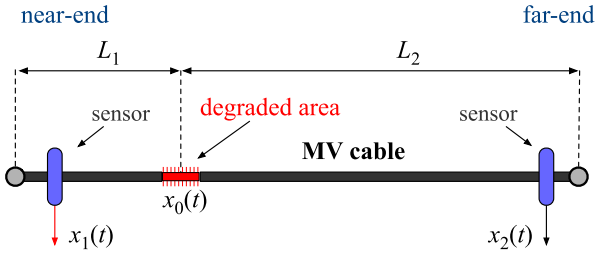

FIGURE 1. Reference model: the PD source is located in the degraded area, L_1 meters from the near-end, and L_2 meters from the far-end. $x_1(t)$ and $x_2(t)$ are the near- and far-end signals, respectively.

$$H(\omega, L) = \exp[-(\alpha_0 + j\beta(\omega))L] \quad \text{where: } \beta(\omega) = \beta_1\omega + 0.5\beta_2\omega^2 \tag{1}$$

In [23], the authors proposed a second order polynomial to model $\beta(\omega)$, to account for the fact that each frequency component travels at a different propagation velocity. β_1 and β_2 are the delay and the dispersion constants, respectively.

Following standard linear analysis, equation (2) provides expressions for the near- and far-end pulses in the multi-path propagation of a PD pulse for the reference model of Fig. 1.

$$\begin{aligned} x_1(t) &= x_0(t) \circledast h(t, L_1) \\ x_2(t) &= x_0(t) \circledast h(t, L_2) + r x_0(t) \circledast h(t, 2L_1 + L_2) \end{aligned} \tag{2}$$

In (2):

a) only the echo produced in the cable near-end has been considered, because attenuation and dispersion will render other echoes negligible (for instance, the echo produced at the far-end);
b) coefficient r models the reflection in the cable near-end, and it is defined as the ratio between the peak-value of the reflected and the incident signals; and
c) $h(t, L_1)$ and $h(t, L_2)$ are the impulsive responses of the equivalent transfer functions $H(\omega, L_1)$ and $H(\omega, L_2)$, respectively ($\circledast$ denotes convolution).

The phase difference $\Delta\Phi$ between signals $x_2(t)$ and $x_1(t)$ in the frequency domain is shown in (3), where Ω is a non-linear term owing to multi-path propagation. Term Ω is detailed in (4), where the coefficient ρ is the effective peak-value of the echo signal shown in (5). The PD signal $x_0(t)$ is assumed to be a gaussian pulse with standard deviation σ_0. The effect of the echo signal is reduced because of both, attenuation (α_0) and dispersion (β_2), as shown in (5).

$$\Delta\Phi = \angle\frac{X_2(\omega)}{X_1(\omega)} = -\beta(L_2 - L_1) - \beta L_1 + \Omega \tag{3}$$

where:

$$\Omega = \text{atan}[(1-\rho)/(1+\rho)\tan(\beta L_1)] \tag{4}$$

$$\rho = r\exp(-\alpha_0 2L_1)(1 + 4\beta_2^2 L_1^2/\sigma_0^4)^{-0.25} \tag{5}$$

Location techniques based on the time domain estimate the PD source location by measuring the difference between TOAs, i.e., the time difference ($\Delta\tau$) that PDs take to arrive

at each cable end, assuming that the captures at both ends are synchronized. On the other hand, those techniques that operate in the frequency domain measure the phase increment $\Delta\Phi$ to estimate $\Delta\tau$.

The time difference $\Delta\tau$ is shown in (6), where $\Delta\Phi'$ is the derivative of the phase difference $\Delta\Phi$ with respect to ω.

$$\Delta\tau = -\Delta\Phi' = \beta'(L_2 - L_1) + \beta' L_1 - \Omega' \tag{6}$$

The first term of (6) is owing to the direct propagation path, whereas the others are due to the near-end echo. Dispersion makes β' to depend on ω. In addition, the non-linear dependence of Ω with ω, due to dispersion and multi-path propagation, is responsible for the performance degradation of location algorithms, both in the time and frequency domains.

To convert a time difference $\Delta\tau$ into a distance, it is necessary to know the propagation velocity v_p, as shown in (7), where $\widehat{L_2}$ is the estimated position of the PDs source measured from the cable far-end, and L is the cable length. Thus, the location error (LE) is calculated using (8).

$$\widehat{L_2} = (\Delta\tau\, v_p + L)/2 \tag{7}$$

$$\text{LE} = L_2 - \widehat{L_2} \tag{8}$$

In a non-dispersive propagation medium, the propagation velocity v_p is equal to β_1^{-1}, but in a dispersive one, every frequency component travels at a different velocity. Therefore, v_p can be computed as an average value, called group velocity, of the PD propagation velocity. A wrong estimation of v_p also produces an error.

Let us now study the effects of dispersion and multi-path propagation on the location error. First, we will consider both situations separately, and then, some simulation results will illustrate their combined effect.

B. EFFECT OF DISPERSION

PD pulses, extremely short at their origin, spread in time duration due to dispersion. Assuming that the PD is modeled as a gaussian pulse with initial deviation σ_0, the resulting pulse deviation σ_L after L meters of propagation is shown in (9) [23]. Using the relationship between the time domain deviation (σ) of a gaussian pulse and its bandwidth (B) shown in (10), we derive (11), that shows the bandwidth reduction of a PD pulse because of dispersion.

$$\sigma_L^2 = \sigma_0^2 + (\beta_2 L/\sigma_0)^2 \tag{9}$$

$$B = \sqrt{2\ln 2}/(\pi\sigma) \tag{10}$$

$$B_0 B_L = \frac{1}{|\beta_2| L}\left(\frac{2\ln 2}{\pi^2}\right) \tag{11}$$

In (11), B_0 is the bandwidth of the initial pulse, and B_L is the resulting bandwidth at L meters from its origin, both calculated in the full-width at half-maximum sense. To derive (11) we assume that $\sigma_0 \ll \sigma_L$.

The reduction of the PD bandwidth caused by dispersion is a key aspect to be considered for an accurate PD location. To illustrate how dispersion reduces the PD bandwidth, Table 1 shows three dispersion scenarios specified by means of the $\beta_2 \times L$ product. An initial deviation $\sigma_0 = 5$ ns is considered, equivalent to an initial bandwidth $B_0 = 75$ MHz. It can be observed that the reduction of the spectral components is significant, especially for the second and third cases. Table 1 also shows the equivalent cable length (L_{eq}), i.e., the length required to achieve the product $\beta_2 \times L$ for a typical dispersion constant $\beta_2 = -0.7\,\text{ns}^2\text{m}^{-1}$, and for the given dispersion case.

TABLE 1. PD Bandwidth (B_L) at the Cable End, Equivalent Length (L_{eq}), and Maximum LE Owing to Dispersion in Three Dispersion Scenarios.

$\beta_2 \times L$ [ns^2]	$B_L^{(a)}$[MHz]	$L_{eq}^{(b)}$[m]	LE$^{(c)}$ [m]
20	58.59$^{(3)}$	28	1.29
100	18.74	142	2.03
500	3.75	714	3.17

$^{(a)}$ Initial pulse bandwidth $B_0 = 75$ MHz ($\sigma_0 = 5$ ns).
$^{(b)}$ Using (11) with $\beta_2 = -0.7$ ns^2/m and $B_0 = 75$ MHz.
$^{(c)}$ Using (12) with $\beta_1 = 5.7$ ns/m, $f = B_L$, and $L_2 >> L_1$.

According to Table 1, in a low dispersion scenario ($\beta_2 \times L = 20\,\text{ns}^2$), PDs propagate a short-distance (tens of meters), and reach the cable ends keeping most of their initial spectral components. In a moderate dispersion scenario ($\beta_2 \times L = 100\,\text{ns}^2$), PDs travel a few hundred meters, reducing their bandwidth to a few tens of MHz. Finally, the high dispersion scenario ($\beta_2 \times L = 500\,\text{ns}^2$) shows how the frequency components of the PD, that propagate between half and one kilometer, are significantly reduced down to a few MHz.

Dispersion also produces small variations in the propagation velocity. For example: for $\beta_1 = 5.7$ ns/m and $\beta_2 = -0.7\,\text{ns}^2\text{m}^{-1}$ (typical values for a XLPE cable [23]), the group velocity is $v_p = \beta_1^{-1} = 175.44\,\text{m}/\mu\text{s}$. But dispersion causes energy components carried around 1 MHz to travel at $175.57\,\text{m}/\mu\text{s}$, while those at 20 MHz travel at $178.19\,\text{m}/\mu\text{s}$.

Expression (12) shows the LE for a single-path propagation model ($r = 0$), assuming a propagation velocity v_p, and a cable dispersion constant β_2.

$$\text{LE} = (L_1 - L_2)2\pi f \beta_2 v_p \tag{12}$$

LE has been evaluated in Table 1 for the three dispersion cases described above. Note that, as shown in Table 1, the maximum frequency that reaches the cable end has been used to compute LE, i.e., $f = B_L$. This value should be considered to be an theoretical lower bound of the LE.

C. EFFECT OF MULTI-PATH PROPAGATION

Non-dispersive multi-path propagation has been widely studied in the radio-communications bibliography [28]. In the model presented above, the near-end reflected signal reaches the far-end cable $2L_1/v_p$ seconds later than the direct-path signal, and both interfere with each other. The resulting signal is affected by frequency selective fading every $\Delta F = (2L_1/v_p)^{-1}$ Hz (commonly called coherent bandwidth). The depth of each fade depends on ρ, i.e., the efective peak-value of the echo signal shown in (5).

The LE in this case is shown in (13), where Ω' (the derivative of Ω with respect to ω) is a non-linear term that strongly depends on ρ, as shown in (4). Function Ω' behaves as a periodic function of the frequency, whose period is ΔF. Although its amplitude depends on ρ, its mean value is L_1/v_p, so that LE $= 0$. Therefore, the position of the PD source can be estimated without error.

$$\text{LE} = (\Omega' v_p - L_1)/2 \tag{13}$$

Under noise conditions, frequency selective fading is responsible for degrading the SNR in some faded frequency components. Location systems should include some processing techniques to cancel these negative effects.

D. COMBINED EFFECT OF DISPERSION AND MULTI-PATH PROPAGATION

The combined effect of both (dispersion and multi-path propagation) can be merged in a single formula (14).

$$\text{LE} = -\frac{1}{2}\{L_1 + v_p[2\pi f \beta_2(2L_2 - L_1) - \Omega']\} \tag{14}$$

This expression has been evaluated for a cable length of 300 m, where PDs are generated in three different positions: 1) close to the cable termination ($L_1 = 5$ m); 2) near the cable end ($L_1 = 50$ m); and 3) in the middle of the cable ($L_1 = 150$ m). In every case the LE is a periodic function of f, with a period ΔF, and its amplitude depends on the effective reduction of the echo peak-value (ρ). The results are shown in Fig. 2 (a), (b), and (c), where the mean value of LE has been evaluated in one period (ΔF).

For non-dispersive propagation, although multi-path propagation causes frequency selective fading, the LE remains zero as shown in Fig. 2. Under dispersion, the worst case is found when the source is very close to one of the cable ends ($L_1 = 5$ m, $L_2 = 295$ m, with $\Delta F = 17.5$ MHz). In this case, shown in Fig. 2(a), both the echo and the direct signals reach the far-end with approximately the same shape (peak-value and pulse-width), and very close in time (57 ns in this example). Dispersion is dominant and severely degrades the location estimate.

For the situation evaluated in Fig. 2(b), the resulting echo signal is distanced 0.47 μs in time (equivalent to a $\Delta F = 1.75$ MHz), and it is dispersed and attenuated more than the direct-path signal. Although the effect of dispersion is still dominant, the degradation can be considered to be acceptable for most cases.

Finally, Fig. 2(c) shows that the LE is negligible for PD sources located in the middle of the cable. In this situation the echo is highly delayed (1.71 μs, yielding to a narrow coherent bandwidth 0.58 MHz), and attenuated with respect to the direct-path signal. In this situation the reflection coefficient r is dominant, but its impact on the LE is negligible.

Fig. 2(d) shows the reduction of the peak-value of the echo signal, relative to the peak-value of the main (or direct) signal due to attenuation and dispersion. This reduction has been evaluated for a reflection coefficient $r = 1$ (the echo-signal is fully reflected). Fig. 2(d) shows that, for a PD source located at $L_1 = 100$ m, the peak-value of the echo is reduced with respect the direct-path signal 7 dB due to attenuation, and 3, 2.4, and 0.4 dB due to dispersion, depending on the $\beta_2 \times L$ product.

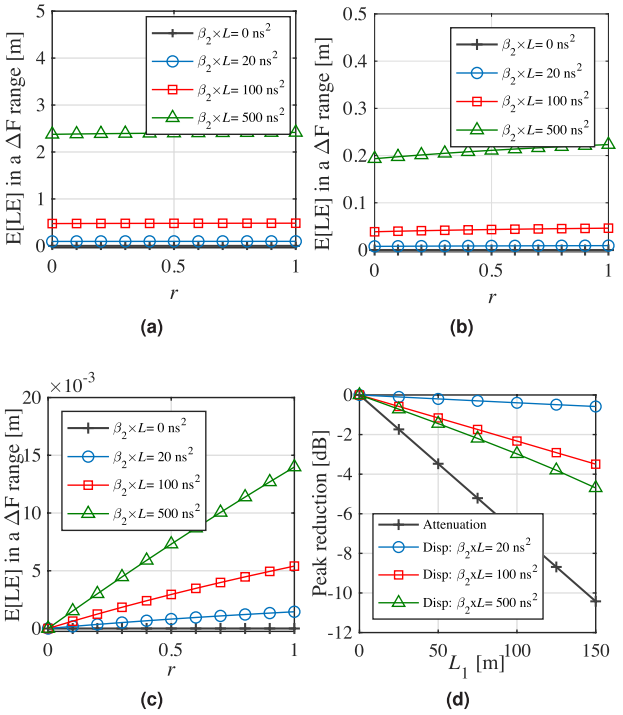

FIGURE 2. Effects of dispersion and multi-path propagation. Subplots (a), (b), and (c) draw the mean value of LE versus the reflection coefficient r for configurations $L_1 + L_2$: (a) 5 m + 295 m, (b) 50 m + 250 m, and (c) 150 m + 150 m. Subplot (d) shows the reduction of the PD pulse peak-value due to attenuation and dispersion, expressed as the peak reduction of the echo signal with respect to the direct signal (the initial pulse deviation is $\sigma_0 = 10$ ns, and the attenuation constant $\alpha_0 = 4 \times 10^{-3}$ m^{-1}).

III. LOCATION TECHNIQUES

The following subsections revise three well-known methods used to estimate the difference between TOAs ($\Delta\tau$). We will focus our attention on the double-ended based location methods, that require both signals to be synchronously captured. Distance L_1 or L_2 (see Fig. 1) can be derived by measuring $\Delta\tau$, as it has been shown in the previous section. $\Delta\tau$ can be measured in the time or the frequency domain.

A. TIME DOMAIN CROSS-CORRELATION (XC)

The discrete XC function $R_{12}(k)$ is defined in equation (15), where $x_1(k)$ and $x_2(k)$ are the discrete-time sequences of $x_1(t)$ and $x_2(t)$, respectively. In a lossless and distortion-free cable, the PD pulse will correlate with itself but not with other independent noise sources. Thus, $R_{12}(k)$ reaches a maximum at $\Delta\tau$, when both signals are best aligned [14].

$$R_{12}(k) = \sum_{m=0}^{1} x_1(m)\, x_2(m+k) \tag{15}$$

The effect of wide-band thermal noise is negligible because it is concentrated at the origin in the XC function, where there is no location information. However, distortion, both in amplitude and phase, multi-path propagation, and other noise sources impact the XC function differently, thereby affecting the estimation of the time difference.

B. FREQUENCY DOMAIN PHASE-INCREMENT (PI)

The phase-increment (PI) between two delayed signals is proportional to the time difference $\Delta\tau$ as shown in (16).

$$\measuredangle X_2(\omega) - \measuredangle X_1(\omega) = -\omega\Delta\tau \tag{16}$$

This well-known Fourier transform property is exploited to estimate $\Delta\tau$. This technique is less influenced by cable dispersion and attenuation, but it is sensible to the phase shift introduced by the load impedance. In the presence of wide-band noise, it is critical to select the frequency range where signals have a good SNR value [13].

Using a discrete Fourier transform of M frequency components, the phase increment $\Delta\theta(m)$ between the near- and far-end sequences $x_1(k)$ and $x_2(k)$ is written in (17), where m denotes the frequency component index. In this article, the PI method estimates $\Delta\tau$ by means of a first order interpolation of the phase increments $\Delta\theta(m)$ at those frequency components that exhibit a significant magnitude.

$$\Delta\theta(m) = -2\pi\, m\, \Delta\tau/(T_s\, M) \tag{17}$$

C. ENERGY CRITERION (EC)

The EC method is based on the computation of the energy-based function of a sequence of N samples $x(k)$, as shown in equation (18), where the first term is the partial signal energy, and the second term is the total signal power. The global minimum of the EC function coincides with the TOA, and it is independent on the noise level [13], [27].

$$\mathrm{EC}(k) = \sum_{m=1}^{k} x(m)^2 - \frac{1}{N}\sum_{m=1}^{N} x(m)^2 \tag{18}$$

IV. SIMULATION RESULTS

A. SIMULATION PROCEDURE

Simulations have been carried out to validate the analyses performed in the previous section, using the reference model of Fig. 1 with typical parameters of a medium voltage cable.

PDs are generated according to the model detailed in [29], where an asymmetric pulse is obtained by means of the summation of a set of gaussian functions. The resulting PD full-width at half-maximum is 19 ns (equivalent bandwidth of $B_0 = 46.45$ MHz). This pulse is propagated towards the cable ends, traveling L_1 meters to the near-end and L_2 to the far-end. The propagation model proposed in [23] was tuned with an attenuation constant $\alpha_0 = 4 \times 10^{-3}\,\mathrm{m}^{-1}$, a delay constant $\beta_1 = 5.7\,\mathrm{ns\,m}^{-1}$, and a dispersion constant β_2 that depends on the dispersion case. In the case of multi-path propagation, an echo signal that propagates from the near- to the far-end was added to the direct-path signal that reaches the far-end cable.

The same additive white gaussian noise power was added to the signals at both cable ends, yielding to different SNR values, SNR_1 and SNR_2, for the near- and the far-end, respectively. The acquired signals were low-pass filtered using a FIR filter with a 3dB cut-off frequency of 40 MHz.

The three location techniques described in the previous section have been modeled. For the PI method, the phase increment is computed for the first 400 components for $\beta_2 \times L$ equal to 0 and $20\,\mathrm{ns}^2$, 200 components for $100\,\mathrm{ns}^2$, and 40 components for $500\,\mathrm{ns}^2$, out of the 16814 available components provided by the Fourier transform. The slope of the PI is calculated by a first-order interpolation.

The location techniques provide a time difference $\Delta\tau$ that is converted to an estimation of the PD source location $\widehat{L_2}$, resulting in LE, as written in (7) and (8), respectively.

We use the following figures of merit to measure the accuracy of location techniques:

- the detection rate for a location error less than 1 m (DR@1m) is the ratio of the number of PDs that have been detected with a LE magnitude smaller than 1 m, out of 1000 simulated PDs. It is plotted versus the SNR.
- the root mean squared (RMS) value of the LE evaluated for $\mathrm{SNR}_2 = -4$ dB, and $\mathrm{SNR}_2 = 6$ dB.

B. SIMULATION RESULTS UNDER DISPERSIVE PROPAGATION

The reference diagram of Fig. 1 has been used with $L_1 = 50$ m, and $L_2 = 450$ m. The DR@1m versus SNR is shown in Fig. 3 for the location techniques under study, and the scenarios detailed in Table 1. Also, the RMS-LE is shown in Table 2 for two SNR_2 values. An analysis of these results is made in the following subsections.

1) XC METHOD

White noise increases the background level of the XC function, but it is necessary a great amount of noise to mask its maximum. The XC method requires an SNR_2 as low as -8 dB to achieve a DR of 90% for a non-dispersive scenario, as shown in Fig. 3(a). These simulation results confirm that the XC method is the best choice for low SNR.

Dispersion makes PD pulses wider in the time domain and, as a result, the XC function presents a flatter shape. Thus, less noise is required to mask its maximum. This effect is especially visible for $\beta_2 \times L = 500\,\mathrm{ns}^2$, where the DR is clearly degraded (an $\mathrm{SNR}_2 = 18$ dB is required to achieve a DR of 90%).

In terms of RMS-LE, XC seems to be the only suitable method to perform PD locations in a very noisy and dispersive environment. The XC method has an RMS-LE of roughly 3 m for $\mathrm{SNR}_2 = -4$ dB in the worst dispersion case, and improves up to 1.25 m for $\mathrm{SNR}_2 = 6$ dB. The LE is negligible for the other dispersion cases.

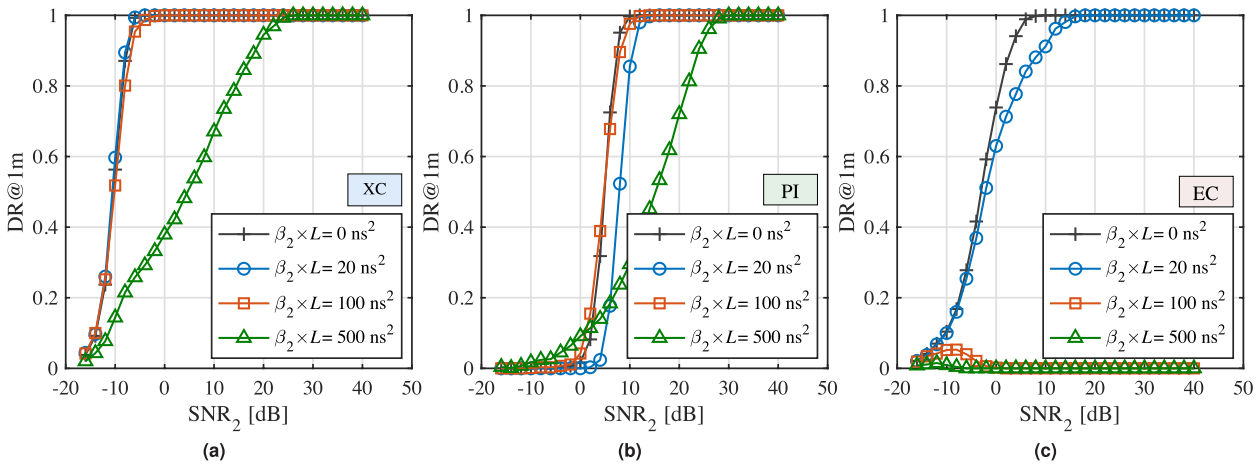

FIGURE 3. Simulation results for dispersive propagation. DR@1m versus SNR at the far-end (SNR$_2$). Three location methods have been simulated: (a) XC, (b) PI, and (c) EC. Dispersion scenarios are specified in legends.

TABLE 2. Simulation Results for Dispersive Propagation: RMS-LE Evaluated in Two SNR Values at the Cable Far-End.

XC:	RMS-LE	
$\beta_2 \times L$	SNR$_2 = -4$ dB	SNR$_2 = 6$ dB
0 ns^2	0.12 m	0.04 m
20 ns^2	0.15 m	0.08 m
100 ns^2	0.39 m	0.16 m
500 ns^2	3.14 m	1.35 m

PI:	RMS-LE	
$\beta_2 \times L$	SNR$_2 = -4$ dB	SNR$_2 = 6$ dB
0 ns^2	50.7 m	5.00 m
20 ns^2	51.3 m	7.31 m
100 ns^2	42.6 m	4.04 m
500 ns^2	37.6 m	4.59 m

EC:	RMS-LE	
$\beta_2 \times L$	SNR$_2 = -4$ dB	SNR$_2 = 6$ dB
0 ns^2	20.4 m	0.21 m
20 ns^2	8.3 m	0.83 m
100 ns^2	16.0 m	4.06 m
500 ns^2	20.8 m	12.7 m

2) PI METHOD

The PI method is more sensitive to white noise than the other location techniques under study. This is due to white noise, which is Gauss-distributed in the time domain, becomes Rayleigh-distributed in the frequency domain. Therefore, the phase of the PD signal in the frequency domain is contaminated by a random component uniformly distributed in $\pm\pi$ owing to noise.

The PI method is also extremely sensitive to the number of spectral components used to perform the location estimation. As propagation attenuates higher frequency components, the SNR decreases in these components. For example, the PI method exhibits better performance for $\beta_2 \times L = 100\,\text{ns}^2$ (see Fig. 3(b)) than for $\beta_2 \times L = 20\,\text{ns}^2$, because the bandwidth used to perform the location in the former is smaller (12.1 MHz) than in the latter (24.2 MHz).

Dispersion reduces the signal captured bandwidth, decreasing the SNR in a significant spectral interval. As a result, the accuracy of the PI method is deteriorated. Fig. 3(b) show that, to achieve a DR of 90%, the PI method requires 7 dB for non-dispersion or low-dispersion, about 11 dB for the moderate dispersion case, i.e., $\beta_2 \times L = 100\,\text{ns}^2$, and 24 dB for the worst dispersion case.

In terms of RMS-LE, the results of Table 2 show that an SNR$_2 = 6$ dB is too low for the PI method to provide acceptable accuracy.

3) EC METHOD

Dispersion produces an asymmetric spread of the pulse: the PD pulse that reaches the far-end is wider than the one that reaches the near-end. Therefore, the minimum of the EC function, i.e., the TOA, is shifted a different time at each end.

Simulation results of Fig. 3(c) show that this method is only valid for non- or low-dispersion scenarios. In these cases, the EC method can provide an acceptable LE. For example, Table 2 shows that the EC reaches an RMS-LE smaller than 1 m for SNR$_2 = 6$ dB.

C. SIMULATION RESULTS UNDER MULTI-PATH PROPAGATION

Now, the scenario of Fig. 1 with $L_2 = 495$ m, and $L_1 = 5$ m, is used to perform simulations in order to evaluate the impact of multi-path propagation on the location accuracy.

An echo is generated in the near-end with a reflection coefficient $r = 0.9$. Thus, the echo signal arrives at the far-end 57 ns delayed ($\Delta F = 17.5$ MHz) with respect to the direct signal. As mentioned above, this is a hostile situation because both signals, echo and direct signal, reach the far-end with approximately the same shape and very close in time.

Two dispersive scenarios have been simulated under gaussian noise conditions: no dispersion ($\beta_2 \times L = 0\,\text{ns}^2$) and moderate dispersion ($\beta_2 \times L = 100\,\text{ns}^2$), both shown in Fig. 4. According to the theoretical analysis previously

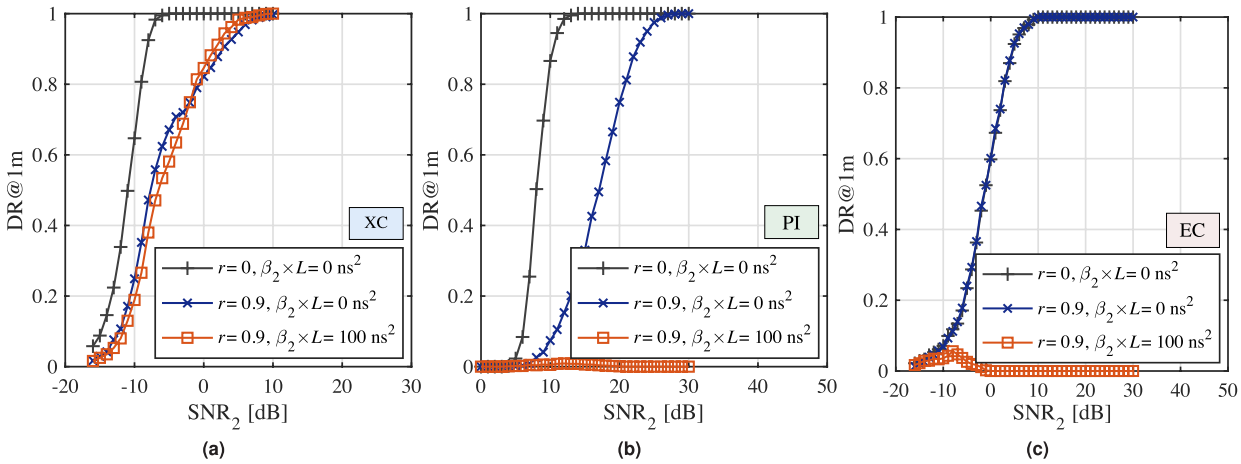

FIGURE 4. Simulation results for multi-path propagation: DR@1m versus SNR at the far-end (SNR_2). Three location methods have been simulated: (a) XC, (b) PI, and (c) EC.

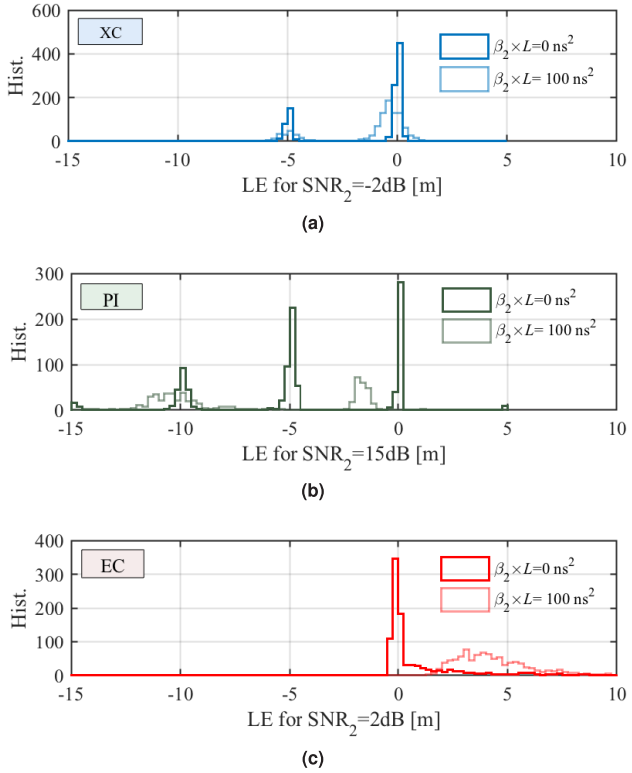

FIGURE 5. Histograms of LE in muti-path scenario for some SNR of interest in two dispersion scenarios. Dark color: no dispersion. Light color: medium dispersion. Location techniques: (a) XC, (b) PI, and (c) EC.

presented, in absence of noise, zero LE is expected for non-dispersion, and about half a meter for $\beta_2 \times L = 100\,\text{ns}^2$. In addition, Table 3 shows the RMS-LE for two SNR_2 values.

The histograms shown in Fig. 5 show the effects of dispersion and multi-path propagation in the location algorithms under study. The following subsections analyze these results.

1) XC METHOD

Multi-path propagation makes the XC function to exhibit several peaks. If only one echo is considered, the XC function will exhibit two peaks. If both, the reflected signal and the noise power are intense enough, the maximum of the XC function will be found at the echo position, rather than at the correct one. The histogram of Fig. 5(a) confirms these two location estimations.

TABLE 3. Simulation Results for Dispersive Multi-Path Propagation: RMS-LE Evaluated in Two SNR Values at the Cable Far-End.

XC:		RMS-LE	
r	$\beta_2 \times L$	$SNR_2 = -4\,\text{dB}$	$SNR_2 = 6\,\text{dB}$
0	$0\,\text{ns}^2$	0.12 m	0.04 m
0.9	$0\,\text{ns}^2$	2.70 m	0.88 m
0.9	$100\,\text{ns}^2$	3.60 m	0.62 m
PI:		RMS-LE	
r	$\beta_2 \times L$	$SNR_2 = -4\,\text{dB}$	$SNR_2 = 6\,\text{dB}$
0	$0\,\text{ns}^2$	50.7 m	5.0 m
0.9	$0\,\text{ns}^2$	74.1 m	23.6 m
0.9	$100\,\text{ns}^2$	68.7 m	36.0 m
EC:		RMS-LE	
r	$\beta_2 \times L$	$SNR_2 = -4\,\text{dB}$	$SNR_2 = 6\,\text{dB}$
0	$0\,\text{ns}^2$	20.4 m	0.21 m
0.9	$0\,\text{ns}^2$	52.1 m	0.58 m
0.9	$100\,\text{ns}^2$	37.5 m	7.46 m

The degradation due to multi-path propagation and noise is shown in Fig. 4(a). For higher SNR values, the XC method provides an accurate location estimation (RMS-LE= 0.88 m for $SNR_2 = 6\,\text{dB}$), as shown in Table 3. To achieve a DR of 90% for multi-path propagation, 3 dB of SNR_2 are required ($-8\,\text{dB}$ in the absence of echo), and, unexpectedly, 2 dB under dispersion, because it reduces the peak value of the echo signal.

Fig. 5(a) shows that dispersion also spreads both signals. The combined effects of dispersion and multi-path propagation produces a displacement in the LE histogram of the peak initially located at LE= 0 (theoretically 0.5 m, as shown in section 2). The RMS-LE for high SNR confirms this LE.

2) PI METHOD

Multi-path propagation is responsible for degrading the performance of the PI method, as shown in Fig. 4(b). In terms of SNR, this degradation is equivalent to 12 dB. To achieve a DR of 90%, an SNR_2 as high as 22.5 dB is required for non-dispersion. This DR cannot be achieved for the dispersion case under study.

The histograms shown in Fig. 5(b) exhibit several peaks at multiples of the echo location due to the periodic nature of the derivative of the phase function Ω under multi-path conditions. The histogram is clearly deteriorated due to dispersion, that shifts the peak initially located at LE = 0 m, with non-dispersion, to somewhere around LE = −2 m. In addition, this peak is spread due to dispersion.

3) EC MEDTHOD

The simulation results of DR depicted in Fig. 4(c), and the histograms of Fig. 5(c) show that EC method is insensitive to multi-path propagation. In terms of RMS-LE, the EC method outperforms the XC method for non-dispersive multi-path propagation.

Simulations also show how the histogram of the LE shifts to a non-zero LE owing to dispersion.

D. DISCUSSION OF RESULTS

Some conclusions can be drawn from the simulations carried out in previous subsections:

1) The XC method is very robust to noise, providing good location accuracy even under high noise conditions. The PI method is especially sensitive to noise and it should be avoided when high noise is expected. Finally, the EC method shows intermediate performances concerning noise.
2) The PI method is extremely sensitive to the number of spectral components used in the computation of the phase increment. Then, when this method is used, especial care is required to select the most appropriate signal bandwidth.
3) The XC and PI techniques can correctly locate PDs even under severe dispersion conditions. On the other hand, the EC method is highly sensitive to dispersion, and it should be avoided even when a moderately high dispersive medium is expected.
4) EC is the only location method which is insensitive to multi-path propagation, but its results hardly compare with those of the XC method.

As a summary, at least under the conditions of this study, the XC method outperforms the rest of techniques under study in nearly every case, including high noise conditions, dispersion and multi-path propagation.

V. CONCLUSION

In this article a new theoretical framework is proposed to understand the impact of propagation on the accuracy of traditional PD location methods. A new expression for the difference of TOAs is proposed that include both, the cable dispersive behaviour and the effects of multipath propagation represented by one echo signal. This expression shows that the difference of TOAs, used to estimate the location of the PD source, depends linearly on the frequency because of dispersion. This dependence becomes non-linear for multi-path propagation. In addition, dispersion reduces the bandwidth of the PDs measured at the cable ends.

The location error in three dispersion scenarios, as well as the worst-case due to multi-path propagation, has been studied for three location methods based on cross-correlation, phase increment, and energy criterion. Simulation results show that the first method outperforms the rest under high noise conditions, even when propagation is affected by dispersion and multipath.

REFERENCES

[1] L. A. Renforth, R. Giussani, M. T. Mendiola, and L. Dodd, "Online partial discharge insulation condition monitoring of complete high-voltage networks," *IEEE Trans. Ind. Appl.*, vol. 55, no. 1, pp. 1021–1029, Jan. 2019.

[2] M. Wu, H. Cao, J. Cao, H.-L. Nguyen, J. B. Gomes, and S. P. Krishnaswamy, "An overview of state-of-the-art partial discharge analysis techniques for condition monitoring," *IEEE Elect. Insul. Mag.*, vol. 31, no. 6, pp. 22–35, Nov. 2015.

[3] A. Milioudis, G. Andreou, and D. Labridis, "On-line partial discharge monitoring system for underground mv cables—Part II: Detection and location," *Int. J. Electr. Power Energy Syst.*, vol. 109, pp. 395–402, Jul. 2019.

[4] A. Madonia, E. R. Sanseverino, P. Romano, I. Troia, S. F. Bononi, M. Albertini, S. Giannini, and G. Mazzanti, "Wireless partial discharge tracking on cross-linked polyethylene MV and HV cables," *IEEE Elect. Insul. Mag.*, vol. 34, no. 6, pp. 8–17, Oct. 2018.

[5] E. W. Shu and S. A. Boggs, "Dispersion and pd detection in shielded power cable," *IEEE Elect. Insul. Mag.*, vol. 24, no. 1, pp. 25–29, Feb. 2008.

[6] J. Jun Guo and S. A. Boggs, "High frequency signal propagation in solid dielectric tape shielded power cables," *IEEE Trans. Power Del.*, vol. 26, no. 3, pp. 1793–1802, Jul. 2011.

[7] A. R. Mor, L. C. C. Heredia, D. A. Harmsen, and F. A. Muñoz, "A new design of a test platform for testing multiple partial discharge sources," *Int. J. Elect. Power Energy Syst.*, vol. 94, pp. 374–384, Jan. 2018.

[8] S. Park and K.-Y. Jung, "Design of a circularly-polarized UHF antenna for partial discharge detection," *IEEE Access*, vol. 8, pp. 81644–81650, 2020.

[9] F.-C. Gu, H.-C. Chang, Y.-M. Hsueh, C.-C. Kuo, and B.-R. Chen, "Development of a high-speed data acquisition card for partial discharge measurement," *IEEE Access*, vol. 7, pp. 140312–140318, 2019.

[10] H. Chai, B. T. Phung, and S. Mitchell, "Application of UHF sensors in power system equipment for partial discharge detection: A review," *Sensors*, vol. 19, no. 5, p. 1029, Feb. 2019.

[11] M. Shafiq, I. Kiitam, P. Taklaja, L. Kutt, K. Kauhaniemi, and I. Palu, "Identification and location of PD defects in medium voltage underground power cables using high frequency current transformer," *IEEE Access*, vol. 7, pp. 103608–103618, 2019.

[12] M. Mahdipour, A. Akbari, P. Werle, and H. Borsi, "Partial discharge localization on power cables using on-line transfer function," *IEEE Trans. Power Del.*, vol. 34, no. 4, pp. 1490–1498, Aug. 2019.

[13] P. Wagenaars, P. A. A. F. Wouters, P. C. J. M. Van Der Wielen, and E. F. Steennis, "Accurate estimation of the time-of-arrival of partial discharge pulses in cable systems in service," *IEEE Trans. Dielectr. Electr. Insul.*, vol. 15, no. 4, pp. 1190–1199, Aug. 2008.

[14] W. L. Weeks and J. P. Steiner, "Instrumentation for the detection and location of incipient faults on power cables," *IEEE Trans. Power App. Syst.*, vol. 101, no. 7, pp. 2328–2335, May 1982.

[15] M. Beyer, W. Kanmm, H. Borsi, and K. Feser, "A new method for detection and location of distributed partial discharges (Cable Faults) in high voltage cables under external interference," *IEEE Trans. Power App. Syst.*, vols. PAS–101, no. 9, pp. 3431–3438, Sep. 1982.

[16] J. P. Steiner, P. H. Reynolds, and W. L. Weeks, "Estimating the location of partial discharges in cables," *IEEE Trans. Electr. Insul.*, vol. 27, no. 1, pp. 44–59, 1992.

[17] R. Mardiana and C. Q. Su, "Partial discharge location in power cables using a phase difference method," *IEEE Trans. Dielectr. Electr. Insul.*, vol. 17, no. 6, pp. 1738–1746, Dec. 2010.
[18] A. Babaee and S. M. Shahrtash, "On-line partial discharge source location in single-core cables with multi sheath-ground connections," *IEEE Trans. Dielectr. Electr. Insul.*, vol. 22, no. 2, pp. 1031–1041, Apr. 2015.
[19] S. Lan, Y. Hu, and C. Kuo, "Partial discharge location of power cables based on an improved phase difference method," *IEEE Trans. Dielectr. Electr. Insul.*, vol. 26, no. 5, pp. 1612–1619, Oct. 2019.
[20] X. Rao, K. Zhou, Y. Li, G. Zhu, and P. Meng, "A new cross-correlation algorithm based on distance for improving localization accuracy of partial discharge in cables lines," *Energies*, vol. 13, no. 17, p. 4549, Sep. 2020.
[21] E. Ouatah, S. Megherfi, K. Haroun, and Y. Zebboudj, "Characteristics of partial discharge pulses propagation in shielded power cable," *Electr. Power Syst. Res.*, vol. 99, pp. 38–44, Jun. 2013.
[22] A. N. Milioudis and D. P. Labridis, "Modelling for on-line partial discharge monitoring on MV cables by using a modified universal line model," in *Proc. IEEE Eindhoven PowerTech*, Jun. 2015, pp. 1–6.
[23] J. Granado, A. Torralba, and C. Álvarez-Arroyo, "Modeling dispersion of partial discharges due to propagation velocity variation in power cables," *Electr. Power Syst. Res.*, vol. 137, pp. 124–132, Aug. 2016.
[24] Y. Tian, B. Qi, R. Zhuo, M. Fu, and C. Li, "Locating partial discharge source occurring on transformer bushing by using the improved TDOA method," in *Proc. Int. Conf. Condition Monitor. Diagnosis (CMD)*, Sep. 2016, pp. 144–147.
[25] Z. Zeng, J. Wang, Y. Hu, Z. Wang, and H. Huang, "Analysis of time-frequency characteristics of pd electromagnetic wave based on electromagnetic simulation," in *Proc. Condition Monitor. Diagnosis (CMD)*, 2018, pp. 1–6.
[26] X. Chen, Y. Qian, Y. Xu, G. Sheng, and X. Jiang, "Energy estimation of partial discharge pulse signals based on noise parameters," *IEEE Access*, vol. 4, pp. 10270–10279, 2016.
[27] M. Mahdipour, A. Akbari, P. Werle, and H. Borsi, "Partial discharge localization on cross-bonded cable systems," *Electr. Power Syst. Res.*, vol. 178, Jan. 2020, Art. no. 106034.
[28] O. Simon Haykin, *Adaptive Filter Theory*, 4th ed. Upper Saddle River, NJ, USA: Prentice-Hall, 2001.
[29] N. Oussalah, Y. Zebboudj, and S. A. Boggs, "Partial discharge pulse propagation in shielded power cable and implications for detection sensitivity," *IEEE Elect. Insul. Mag.*, vol. 23, no. 6, pp. 5–10, Nov. 2007.

JOAQUÍN GRANADO was born in Córdoba, Spain, in 1973. He received the master's and Ph.D. degrees in telecommunication engineering from the Universidad de Sevilla, in 1999 and 2005, respectively. He is currently with the Electronic Engineering Department, Universidad de Sevilla. His research interests include signal processing, modeling, measuring, and instrumentation for partial discharges and communications systems.

ANTONIO TORRALBA (Senior Member, IEEE) received the M.Sc. degree in electrical engineering (industrial engineering) and Ph.D. degrees from the Universidad de Sevilla, Spain, in 1983 and 1985, respectively. He was a Visiting Researcher with the Klipsch School of Electrical Engineering, New Mexico State University, Las Cruces, USA, in 1999, and also with the Department of Electrical Engineering, Texas A&M University, College Station, USA, in 2004. He is currently with the Department of Electronics Engineering, where he is currently a Professor and also with the Laboratory of Engineering for Energy and Environmental Sustainability, Universidad de Sevilla, where he also leads a research group on mixed signal design.

He has coauthored 90 articles in international journals. His research interests include low-power low-voltage analog and mixed-signal microelectronics.

CÉSAR ÁLVAREZ-ARROYO was born in Granada, Spain, in 1979. He received the master's and Ph.D. degrees in electrical engineering from the Universidad de Sevilla, in 2009 and 2019, respectively. His current research interest includes partial discharges in cables.